Article

Portable Raman Spectrometer for In Situ Analysis of Asbestos and Fibrous Minerals

Jasmine Rita Petriglieri [1,2,*], Danilo Bersani [3], Christine Laporte-Magoni [4], Mario Tribaudino [5], Alessandro Cavallo [6], Emma Salvioli-Mariani [5] and Francesco Turci [1,2]

[1] "G. Scansetti" Interdepartmental Centre for Studies on Asbestos and Other Toxic Particulates, University of Torino, Via Pietro Giuria 7, 10125 Torino, Italy; francesco.turci@unito.it

[2] Department of Chemistry, University of Torino, Via Pietro Giuria 7, 10125 Torino, Italy

[3] Department of Mathematical, Physical and Computer Sciences, University of Parma, Parco Area delle Scienze 7/A, 43124 Parma, Italy; danilo.bersani@unipr.it

[4] Institute of Pure and Applied Sciences, Université de la Nouvelle Calédonie, Campus de Nouville, BP R4, Nouméa 98851, New Caledonia; christine.laporte@unc.nc

[5] Department of Chemistry, Life Sciences and Environmental Sustainability, University of Parma, Parco Area delle Scienze 157/A, 43124 Parma, Italy; mario.tribaudino@unipr.it (M.T.); emma.salviolimariani@unipr.it (E.S.-M.)

[6] Department of Earth and Environmental Sciences, University of Milano-Bicocca, Piazza della Scienza 4, 20126 Milano, Italy; alessandro.cavallo@unimib.it

[*] Correspondence: jasminerita.petriglieri@unito.it

Featured Application: Portable Raman can detect asbestos and asbestos-like minerals in the field.

Abstract: Asbestos inhalation is associated with fatal respiratory diseases and raises concerns from the perspective of workplace safety and environmental impacts. Asbestos and asbestos-like minerals naturally occur in rocks and may become airborne when outcrops or soils are disturbed by anthropic activities. In situ detection of these minerals is a crucial step for the risk evaluation of natural sites. We assess here whether a portable Raman spectrometer (pRS) may be used in the identification of asbestos and asbestos-like minerals at the mining front during exploitation. pRS performance was tested at three geologically different mining sites in Italy and New Caledonia and compared with a high-resolution micro-Raman spectrometer (HRS). About 80% of the overall in situ analyses at the mining front were successfully identified by pRS, even when intermixed phases or strongly disaggregated and altered samples were analyzed. Chrysotile and tremolite asbestos, asbestos-like antigorite, and balangeroite were correctly detected during surveys. The major difficulties faced during in situ pRS measurements were fluorescence emission and focussing the laser beam on non-cohesive bundles of fibers. pRS is adequate for discriminating asbestos and asbestos-like minerals in situ. pRS may support risk assessment of mining sites to better protect workers and environment.

Keywords: portable Raman; micro-Raman; asbestos; fibrous antigorite; balangeroite; environmental monitoring; mining

1. Introduction

The occurrence of natural deposits of asbestos and other potentially hazardous fibrous minerals poses concerns for occupational and environmental exposure (e.g., [1–3]). Asbestos refers to a commercial and regulatory designation applied to a group of six silicate minerals belonging to the mineralogical family of serpentine (chrysotile) and amphiboles (amosite, crocidolite, anthophyllite, tremolite, and actinolite; [4] and European Union (EU) Directive 2003/18/EC). Other non-asbestos mineral fibers, including

the zeolite erionite and the amphibole fluoro-edenite, were also proved to be able to induce human mesothelioma and were classified as carcinogenic to humans by the International Agency for Research on Cancer [4,5]. Whether unregulated fibrous minerals pose a hazard to humans and the environment is a matter of debate [6,7]. Recently, several environmental and health agencies worldwide (e.g., The National Institute for Occupational Safety and Health, NIOSH [8]; International Association for Engineering Geology and the Environment, IAEG Commission [9]; National Institute for Insurance against Accidents at Work, INAIL [10]; Agence Nationale de Sécurité Sanitaire de l'Alimentation, de l'Environnement et du Travail, ANSES [11]) focussed their attention on the assessment of the hazard of fibrous minerals which share with asbestos physicochemical properties relevant to toxicity. Several potentially hazardous asbestos-like minerals were or are currently under investigation: fibrous antigorite [12], balangeroite [13,14], fibrous glaucophane–winchite [15,16], fibrous ferrierite [17], and fibrous mordenite [18] have been investigated in the past years.

The occurrence of fibrous, elongated mineral particles (EMP) in natural settings may have a significant impact, especially on mining and quarrying operations [6], where EPM-bearing rocks and soils are exposed and manipulated by exploitation activity (e.g., excavation, crushing, sieving, transportation, waste management), potentially increasing the risk to human exposure [19–21].

Asbestos-bearing occurrences are complex mineralogical environments, characterized by the intergrown of different mineral varieties occurring in a wide range of morphologies (e.g., [22]). Quantification of the occurrences of EMPs represents a crucial step for the risk evaluation of natural sites where fibrous minerals may occur. However, to obtain a significative quantitative analysis of EMP in rocks [23–25], an in situ screening of the presence of asbestos and asbestos-like minerals at the excavation front must be carried out. In this context, portable equipment able to distinguish potentially hazardous minerals from other non-hazardous varieties is highly envisaged. This work was designed to test the in situ performance of Raman spectroscopy in the characterization of mineralogical assemblage at the outcrop.

The spectroscopic assignment of minerals by infrared spectroscopy and micro-Raman spectroscopy is today reliable on both rock specimens (rock fragments and petrographic thin sections; [26–28]) and asbestos-containing materials [29,30]. Confocal micro-Raman has an intrinsic higher spatial resolution (up to 1 μm on xyz directions with conventional benchtop setups) than micro-IR, and this makes Raman spectroscopy particularly suitable to discriminate intergrown species that are often found in serpentine and amphiboles rich outcrops. Raman spectra are very sensitive to variations in chemical composition and structure, allowing the discrimination of the different mineral phases [31–34]. Micro-Raman allows the synergic exploitation of the structural discriminating power and the small portion of the investigated sample to extend the use of Raman spectroscopy to micrometric fiber bundles and/or single micrometre-sized fibers (fiber of 1–2 μm in diameter; [35,36]). Such exceptional instrumental properties were also exploited in the detection of mineral fibers in histological specimens [37,38]. However, delicate optics, hazardous high-power laser sources, and a heavy anti-vibration table and electronics characterize benchtop setups. To take advantage of the highly diagnostic power of Raman spectroscopy during in situ surveys, portable instruments were tested in the identification of asbestos and asbestos-like minerals at the outcrop [36,39]. However, a work devoted to comparatively test the performance of portable Raman spectroscopy (pRS) under different environmental and geological conditions is still lacking.

This work aims to evaluate the capabilities of pRS in the identification and discrimination of asbestos and asbestos-like minerals in three mining sites differing in the geological setting and associated minerals. A comparison with benchtop high-resolution micro-Raman spectrometer was carried out to estimate the performance, advantages, and instrumental limitations of the portable Raman.

The use of a portable Raman may help professional geologists involved in the health and safety assessment of mining sites to protect workers and the environment better.

2. Materials and Methods

2.1. Description of Investigated Area

To test the possible interference of rock fabric (i.e., matrix) on the diagnostic power of portable Raman, three different kinds of industrial exploitation sites occurring in different geological settings, namely an active serpentine quarry (Valmalenco, Italy; Figure 1a), a former asbestos chrysotile mine (Balangero mine, Italy), and an active Ni-ore lateritic deposit (Tontouta mine, New Caledonia, Figure 1b) have been selected. Particular attention was devoted to assessing if the degree of cohesion of hosted rocks (from massive serpentine to lateritic soil) and the presence of secondary phases (e.g., chlorite, saponite, diopside) in the mineralogical matrix should affect the quality of spectra.

The Valmalenco area (central Alps, northern Italy, Figure 1a) is located at the Penninic to Austroalpine boundary zone, and the most important tectonic unit is the Malenco-Forno nappe, a huge ultramafic body (more than 130 km^2) interpreted as a sub-continental mantle fragment [40,41]. The most common lithotype is represented by schistose antigoritic serpentinites, consisting of antigorite, olivine, diopside, and minor magnetite and chlorite, and quarried as valuable dimension stone and marketed worldwide [42]. These serpentinites also host different industrial mineral deposits, ranging from talc lodes up to long-fiber chrysotile veins. Moreover, well-formed demantoid crystals, a Cr-rich variety of andradite garnet, may occur in chrysotile veins [43]. Asbestos, which occurs in discrete cross-fiber and slip-fiber veins, gave rise in the past to widespread mining activity, particularly between the end of the XIX century and 1975, and was used mainly for weaving tablecloths or for wicks.

The Balangero chrysotile mine (western Alps, Piedmont, northern Italy) was the biggest asbestos mine in Europe: the extraction started in 1923, peaking in the seventies and eighties (up to 1.5×10^6 m^3 of tout-venant per year), and stopped definitively in 1990. The chrysotile mineralization (both cross-fiber and slip-fiber) is hosted by the ultramafites (upper mantle tectonites) of the Balangero body and the adjacent Lanzo massif (Internal Piedmontese Zone, Penninic Domain), partly re-equilibrated by the early-alpine high pressure–low temperature metamorphism (500–550 °C, 15 kb) into antigoritic serpentinites [44,45]. Therefore, two generations of chrysotile veins occur [46]. The first vein generation consists of long-fiber chrysotile (up to several centimeters in length). The second vein generation consists of short-fiber chrysotile (a few millimeters in length). Other fibrous minerals (e.g., balangeroite) are associated with chrysotile asbestos in the orebody.

The Tontouta-Opoué open mine (Massif du sud, southwest New Caledonia; Figure 1b) is set in Ni-rich lateritic deposits formed by pedogenesis of exposed ultramafic protolith. Ni-laterite deposits were formed during the Neogene by lateritic weathering of obducted and serpenized harzburgite–dunite peridotite [47–50]. Serpentine minerals (chrysotile, fibrous antigorite) and minor tremolite–actinolite amphiboles are commonly hosted in lateritic and saprolitic zone currently mined [51]. As a consequence of pedogenetic processes, Caledonian samples show a peculiar strongly fibrous appearance. At the hand scale, rock fragments appear more friable and with a structureless aspect.

2.2. Samples

Representative asbestos-bearing veins and massive rock samples have been collected during the three in situ surveys to perform the comparison with the high-resolution micro-Raman spectrometer. Due to the high number of literature works describing the paragenesis of serpentinites hosting asbestos-bearing mineralization of the sites, only a brief minero-petrographic description of representative asbestos veins is provided (Figure 2 and Supplementary Materials S2).
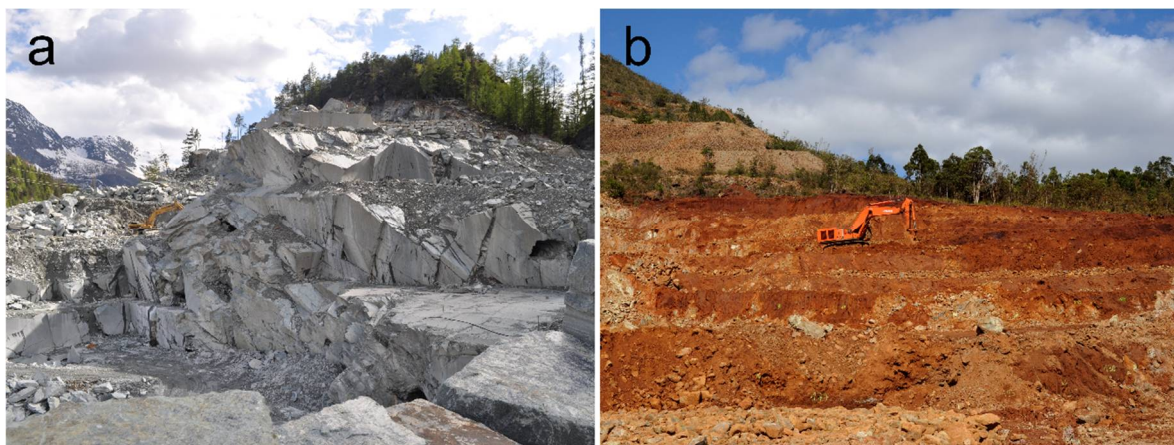
Figure 1. Mining sites. (**a**) Serpentine quarry at Valmalenco (central Alps, northern Italy); (**b**) Ni-open pit of Tontouta (Massif du sud, New Caledonia).

2.3. Mineralogical Investigation

Rock and mineralized vein samples were identified and chemically characterized by polarized light microscopy (PLM) on thin sections, X-Ray powder diffraction (XRPD), and scanning electron microscopy associated with energy dispersive X-Ray spectroscopy (SEM-EDS).

The bulk mineralogy was determined by qualitative XRPD analysis using: (i) for Balangero samples, Rigaku Miniflex 600 diffractometer; (ii) for Valmalenco samples, PANalytical X'Pert PRO PW3040/60 diffractometer; and (iii) for Caledonian samples, Bruker-AXS D8 Advance diffractometer equipped with an Si(Li) solid-state detector. Intensity measures were run at 40 kV and 15–40 mA, using CuKα radiation (λ = 1.54178 Å) over a 2θ range from 3 to 80° 2θ in steps of 0.02°, with a counting time of 1 s per step. The limit of detection of XRPD depends on the mineral phase and is generally comprised between 0.1 wt% for highly crystalline phases and 5 wt%; for serpentine minerals, it is usually 1 wt%. Representative diffraction patterns are reported in Supplementary Materials S2.

Sample morphology and semi-quantitative EDS microanalysis were investigated on natural samples and thin sections using: (i) Zeiss Evo50 SEM for Balangero samples; (ii) Vega TS Tescan 5163 XM in combination with EDAX Genesis 400 analyzer for Valmalenco samples; and (iii) JEOL JSM-IT 300 LV/LA with Low Vacuum Mode equipped with an Oxford-X-Max EDS for Caledonian samples. Secondary Electron Images were acquired at various magnifications and accelerating voltages, commonly 3–10 kV or 20 kV with 90 pA or 200 pA.

2.4. Raman Investigation

Raman in situ measurements were carried out with a portable Enspectr RaPort® Raman spectrometer (pRS), a 'pistol-like' handheld instrument weighing 2.1 kg, equipped with a thermoelectrically cooled silicon Charge-Coupled Device and a 532-nm laser at a maximum output power of 30 mW. The laser spot is nearly 0.5 mm (Figure S1, Supplementary Material). Raman spectra were obtained in the extended wavenumber range 100–4000 cm^{-1} with a spectral resolution of 8 cm^{-1}. The instrument is controlled remotely via a USB 2.0 cable connected to a laptop. It allows the operator to select settings for measurements, including more detailed power output selection, number of accumulations, and long accumulation times. The spectra were collected in a single acquisition up to 60 s. The instrument calibration was checked against the position of the bands of reference materials before each set of measurements. A working time up to 6 h at temperatures between 0 °C and 40 °C is recommended. For a comparison with other portable Raman instruments, see Jehlička et al. (2017) [52].
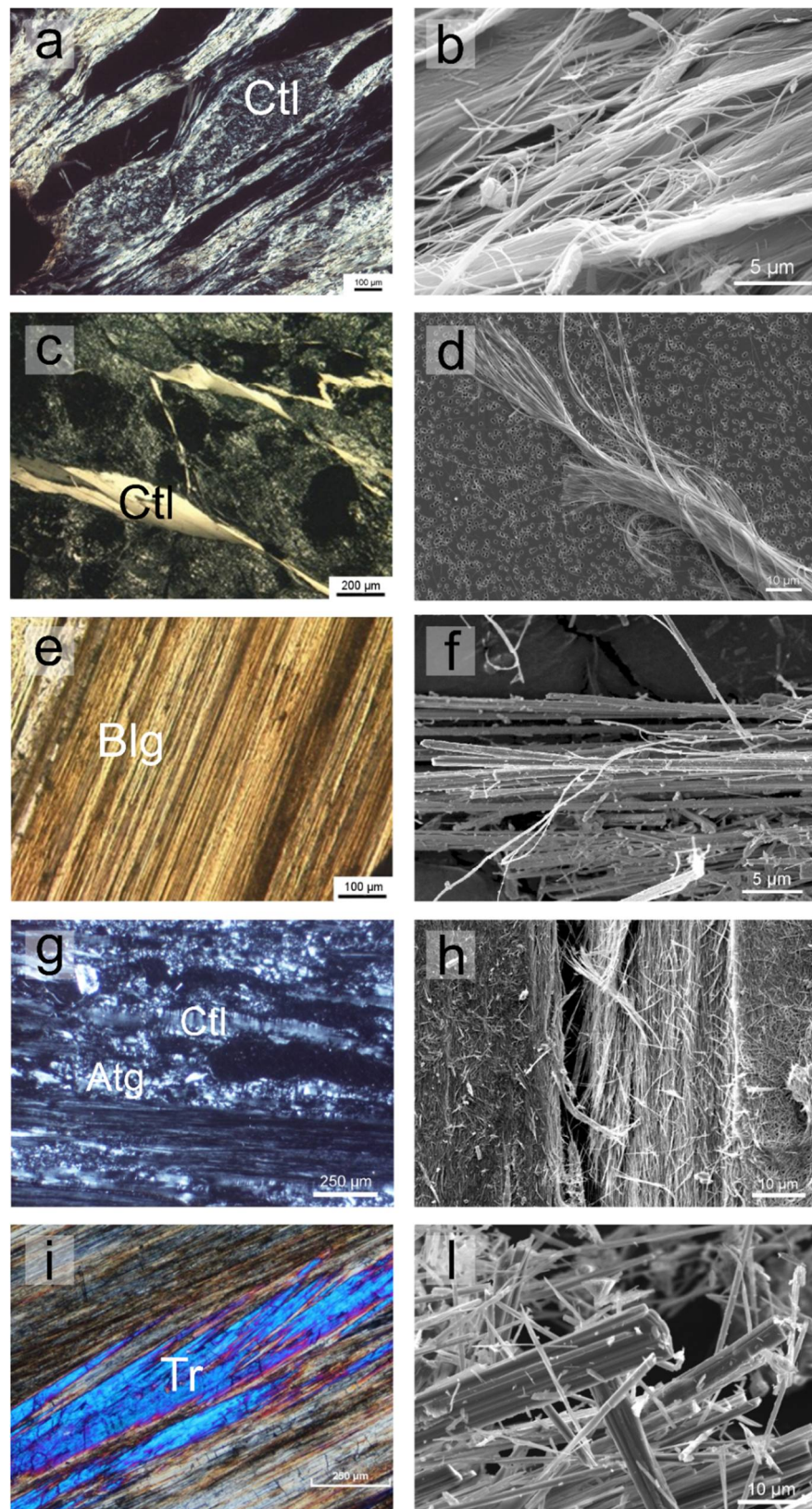
Figure 2. Petrographic and morphological (SEM images) description of representative NOA-bearing samples. Optical photomicrographs (cross-polarized light images on the left) and SEM images (on the right) showing: (**a**,**b**) Valmalenco quarry. Veins of slip long-fiber chrysotile; (**c**,**d**) Balangero mine. Veins of slip chrysotile; (**e**,**f**) Balangero mine. Bundle of balangeroite fibers; (**g**,**h**) Tontouta Ni-open pit. Bundle of chrysotile and fibrous antigorite; and (**i**,**l**) Tontouta Ni-open pit. Bundle of tremolite fibers. Abbreviations: Ctl, chrysotile; Blg, balangeroite; Atg, antigorite; Tr, tremolite.

High-resolution micro-Raman (HRS) spectra were acquired on rock fragments and petrographic thin sections in nearly backscattering geometry with a Horiba Jobin-Yvon LabRam apparatus, equipped with an Olympus microscope with 10×, 50×, Ultra-Long Working Distance 50×, and 100× objectives and a motorized x-y stage, and a holographic grating with 1800 lines/mm. The 473.1-nm line of a doubled Nd: YAG diode pumped laser was used as excitation; laser power was controlled by means of a series of density filters to avoid heating effects. The minimum lateral resolution was about 1 μm (with the 100× objective); the depth resolution was set to a few microns by means of a confocal hole. The spectral resolution was about 4 cm^{-1}. The system was calibrated using the 520.7 cm^{-1} Raman peak of silicon before each experimental session. In addition, in the high wavenumber range, spectra were constantly calibrated using spectral lamps. Spectra were collected using the 100× objective with repeated acquisition: 5 acquisitions for 30 s and 15 for 10 s in the low and high wavenumber spectral range, respectively.

The background subtraction on each spectrum was performed with LabSpec® software.

3. Results and Discussion

3.1. Mineralogical Description

Valmalenco asbestos-bearing veins mainly consist of long-fiber chrysotile, occurring in sub-vertical cross-fiber and slip-fiber veins, with thickness from mm up to several cm [42]. XRPD analysis of mineralized veins confirmed the sole presence of serpentine (Supplementary Material S2.1). Under the microscope, veins of slip chrysotile occur in the form of bundles of fibrous and curvilinear fibers, typical of the chrysotile morphology (Figure 2a,b).

In the former Balangero asbestos mine, where massive and fractured serpentinites occur, two generations of both short (Figure 2c,d) and long-chrysotile veins crop out in the northern part of the mine. An example of slip short-fiber chrysotile veins is displayed in Figure 2c. Balangeroite was strictly associated with longer fiber chrysotile veins (Figure 2e). XRPD analysis showed the presence of serpentine associated with magnetite (Supplementary Material S2.2 and S2.3). Minor amounts of stichtite (chromium and magnesium carbonate; Supplementary Material S2.2) and balangeroite (Supplementary Material S2.3) were detected. At SEM observation, chrysotile presents its peculiar morphology, characterized by bundles of fibrous, curvilinear thin fibers with frayed and splayed ends (Figure 2d). Balangeroite occurs in the form of a bundle of rigid acicular elongated particles (Figure 2e,f) due to its gageite-like structure [53].

At the Tontouta mine, veins of chrysotile and fibrous antigorite, with thickness from less than 1 mm to several centimeters, were intimately associated with minor tremolite–actinolite amphiboles. XRPD analysis of mineralized serpentine (Supplementary Material S2.4) and tremolite (Supplementary Material S2.5) veins confirmed the identification of the main phases. Minor chlorite, talc, and other Mg-Al-rich phyllosilicate (e.g., saponite) were occasionally observed. Petrographic and SEM observations showed the intimate intergrowth of chrysotile and fibrous antigorite fibers to form curvilinear bundles (Figure 2g,h). Tremolite occurred in highly fractured veins, with an acicular to needle-like morphology (Figure 2i,l).

3.2. In Situ Identification of Asbestos and Fibrous Minerals

Results of in situ tests realized with pRS at the mining front are summarized in Table 1. Tests performed on asbestos-bearing veins allowed the discrimination of asbestos (e.g., Valmalenco quarry, Italy), also where asbestos chrysotile and asbestos tremolite phases were intergrown (e.g., Tontouta mine, New Caledonia). Among non-asbestos fibers, Raman spectra of fibrous antigorite, saponite, and balangeroite were recorded (Table 1). When tested on peridotite matrix in Balangero mine, pRS allowed the identification of the

typical mineralogical association of the site, consisting of antigorite, lizardite, chlorite, (fibrous) diopside, and olivine (Table 1 and Supplementary Material S3).

Table 1. Overview of the Raman spectra performed at the exploitation sites of Valmalenco (central Alps, Italy), Balangero (western Alps, Italy), and Tontouta (Massif du sud, New Caledonia). Portable Raman spectrometer (pRS) allowed the identification of asbestos and asbestos-like minerals in the low- to highly-altered peridotite matrix. Raman spectra of non-asbestos or asbestos-like minerals are reported in Supplementary Material S3.

Mining Site	Spectral Quality *	Detected Mineral Phases										
		Tr	Ctl	Atg (Fibrous)	Lz	Blg	Di (Fibrous)	Chl	Sap	Ol	Grt	Mixed Phases
Valmalenco	90%		6	2							1	
Balangero	84%		6	8	3	3	5	3		1		3
Tontouta	70%	3	5	11					2	1		1

* Spectral quality = number of analyses with sufficient quality to distinguish mineral phases/number of total analyses performed × 100. Abbreviations: Tr, tremolite; Ctl, chrysotile; Atg, antigorite; Lz, lizardite; Blg, balangeroite; Di, diopside; Chl, chlorite; Sap, saponite; Ol, olivine; Grt, garnet.

To assess if the degree of cohesion of rock specimens may affect the performance of pRS, Raman spectra collected on differently cohesive veins, from massive to friable-powdered material, were compared. As shown in Figure 3, the progressive loss of cohesion of selected specimens did not affect data quality, and antigorite and tremolite phases were identified (Figure 2a and Figure 2b, respectively). Spectra from in situ surveys with pRS were compared with literature data, and a good agreement with the main spectral features, i.e., peak position (wavenumber), shape, and relative intensity at both low- and high-wavenumber regions was observed [26,53] (Supplementary Material S4).

About 80% of the overall spectra collected in the three sites with pRS were of sufficient quality to allow a successful identification of the mineral phase(s) interacting with the laser beam. To quantify this important instrumental parameter, that we called "spectral quality", we calculated the percentage ratio between the number of analysis acquired with the sufficient quality to distinguish the mineral phases and the total number of analysis performed (n. of analyses at Valmalenco 10, Balangero 37, Tontouta 33). This allowed us to draw a first evaluation of the instrumental capabilities during in situ asbestos monitoring (Table 1). The lower spectral quality was registered during the Tontouta survey, with about 70% of the spectra resulting in assignable plots, while the quality of the spectra collected during the Valmalenco and Balangero surveys was 90% and 84%, respectively. This result may be ascribed to several factors: (i) the fluoresce phenomena, due to the host rock interference is likely higher at Tontouta mine, where Fe-rich lateritic soil may induce a higher fluorescence effect; (ii) the chances to correctly focus the laser beam on the rock is lower at Tontouta mine, where non-cohesive bundles of altered fibers were more commonly observed than at the other two sites.

3.3. Evaluation of the Performance of pRS

Raman spectra recorded with pRS were compared with spectra obtained with benchtop high-resolution micro-Raman spectrometer (HRS). A comparison of different working conditions is reported in Table 2. HRS was used on petrographic polished thin cross-sections, optimizing the working conditions, such as spot analysis, objective, filter, time, and number of acquisitions, to obtain the best spectra virtually achievable with the given instrument. It is worth noting that pRS used for this work does not allow for fine-tuning the instrumental parameters, but the time of acquisition only.
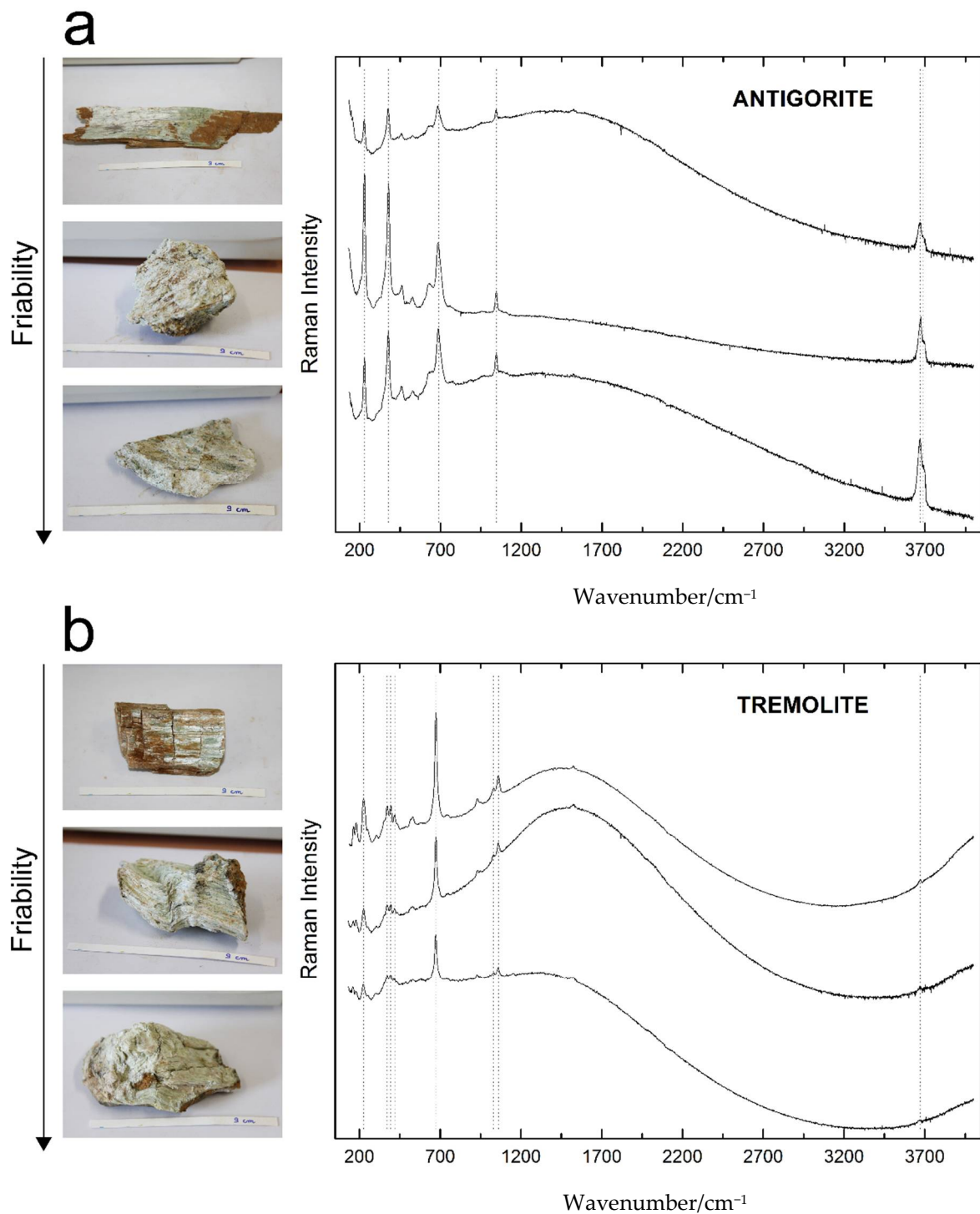
Figure 3. Estimation of performance of portable Raman on differently cohesive, from massive to friable-powdered, asbestos-bearing veins from Tontouta Ni- open pit mine. (**a**) antigorite; (**b**) tremolite. Raman spectra were acquired in the extended spectral region (100–4000 cm^{-1}).

Table 2. Working conditions of portable Raman device (on the left) compared to benchtop high-resolution micro-Raman spectrometer (on the right).

Portable Equipment	Micro-Raman
on bundles of fibers	on thin section
on an irregular surface	on a polished surface
pre-set measuring conditions	optimal measuring conditions
laser source 532 nm (green)	laser source 473.1 nm (blue)
spatial resolution 1 mm	spatial resolution 1–2 μm
spectral resolution 8 cm^{-1}	spectral resolution 4 cm^{-1}

In Figure 4, spectra of chrysotile, fibrous tremolite, fibrous antigorite, and balangeroite collected with pRS and HRS are compared. Despite obvious differences in signal-to-noise ratio and spectral resolution (8 cm^{-1} and 4 cm^{-1}, respectively), Raman spectra showed very similar profiles at both low- (100–1800 cm^{-1}) and high-wavenumber (3500–3800 cm^{-1}) regions. The presence of the diagnostic features in the OH-stretching region (3500–3800 cm^{-1}), with the main peaks located at about 3698 cm^{-1} for chrysotile, 3668 and 3695 cm^{-1} for antigorite [33], 3672 cm^{-1} for tremolite [54], and 3670 cm^{-1} for balangeroite [55], allowed the discrimination among fibrous mineral phases easily. The OH stretching peaks in high wavenumbers were often partially covered by fluorescence interference. The annoying effect of fluorescence was particularly evident in spectra obtained with pRS for tremolite samples (Figures 2b and 4c). Nevertheless, the identification of the asbestos-tremolite variety as the predominant phase was not compromised due to the well-resolved low-frequency pattern.

Due to the intimately mixed nature of asbestos-type occurrences, even at the sub-micron scale, some level of contamination due to the simultaneous interaction of the laser beam with crystals of several mineral phases is likely to occur. Obtaining informative spectra on mixed-mineral varieties is rather challenging. In the case of finely intermixed phases (Figures 5 and Supplementary Material S5), the superimposed contributions due to the Raman scattering of antigorite and chrysotile phases were clearly observed (Supplementary Material S5). At low-wavenumbers, the spectrum was dominated by the Raman bands associated with chrysotile, even if the occurrence of the shoulder at 380 cm^{-1} and the peaks at 625 and 1045 cm^{-1} suggested the presence of antigorite phase. At higher wavenumbers, the doublet associated with OH-stretching vibrations showed an intermediate shape between chrysotile and antigorite varieties. When multiple phases occurred, simply increasing the number of acquisitions may ensure the detection not only of the main mineralogical phase but also the occurrence of secondary phases present in minor amounts.
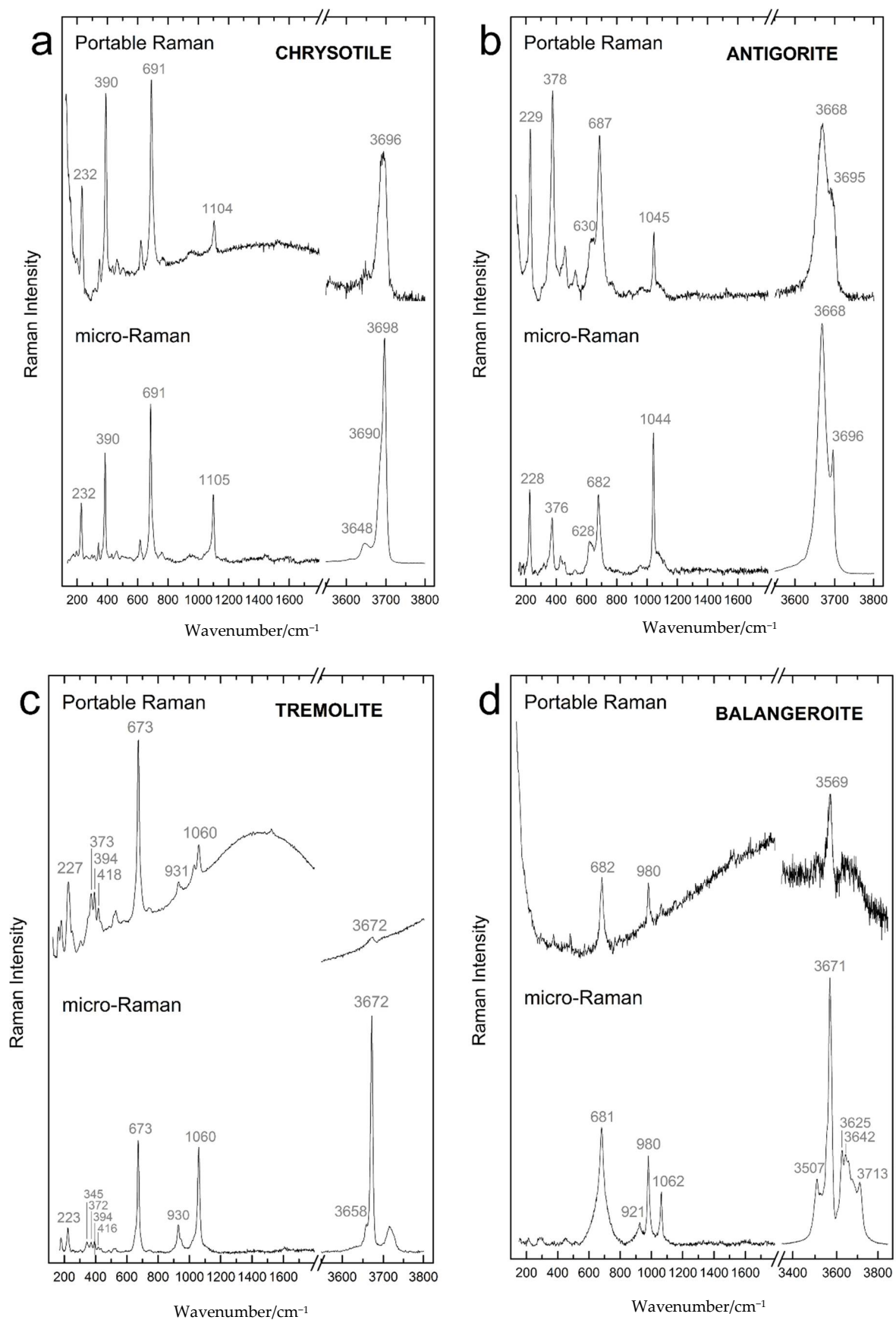
Figure 4. Comparison of Raman spectra of (**a**) chrysotile; (**b**) antigorite; (**c**) tremolite, and (**d**) balangeroite collected with portable Raman (on the top) and micro-Raman spectrometer (on the bottom).
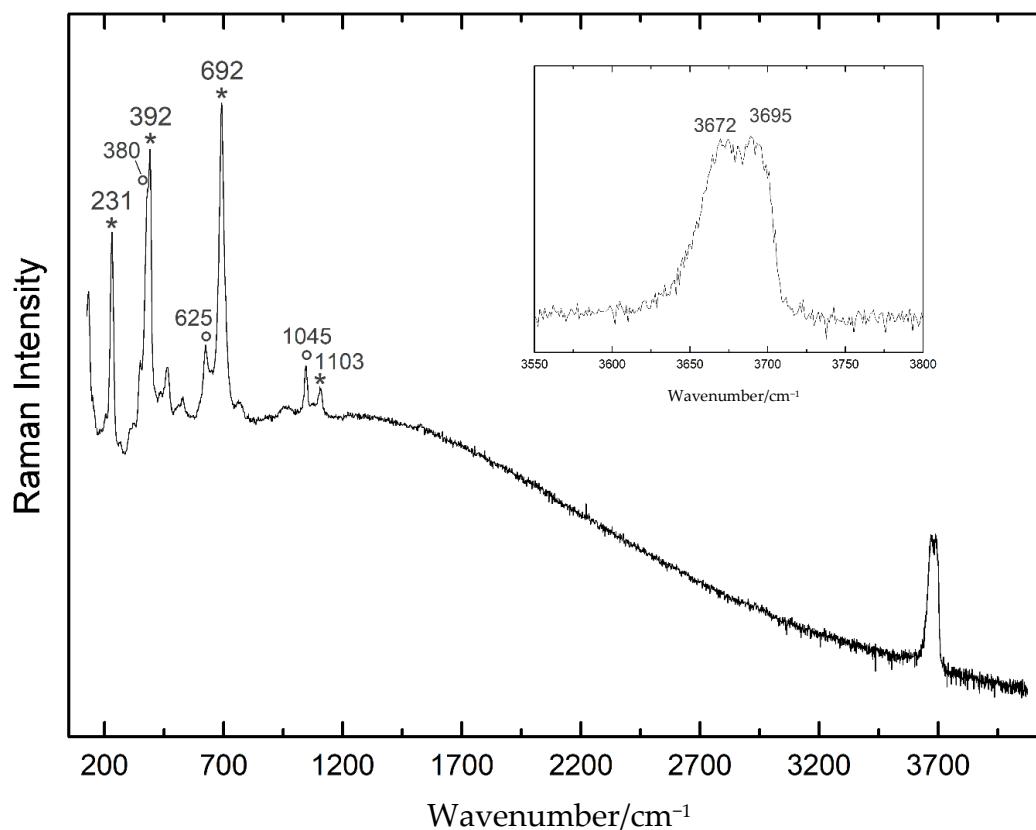
Figure 5. Raman spectra of a bundle consisting of chrysotile (circle assignment) and fibrous antigorite (asterisk assignment) collected with portable Raman. The contribution of OH-stretching of the two phases occurred simultaneously. A comparison with Raman spectra collected with HRS is reported in Supplementary Material S5.

Taking into account the larger laser spot (about 1 mm, versus 1–2 μm of HRS) and the lack of rigid mount for positioning samples, the real spatial resolution of portable Raman was estimated in the order of a cubic millimeter. This could be a disadvantage when analyzing very small features, but it allows the detection of mixed-mineral varieties.

This multi-site experimental approach evidenced that the main parameters that may affect the spectral quality of spectra collected with pRS are the possible difficulty of focusing the laser beam on non-cohesive and irregular surfaces and the fluorescence interference. According to Zohlobenko et al. (2020), the nature of the matrix may affect the identification of asbestos and asbestos-like minerals. In the present study, the nature of rock fabric, consisting of massive to friable-powdered rocks formed by complex mineralogical associations (mixed aggregates of mineral fibers at the micro or sub-micro scale), slightly impacted the spectral quality.

pRS was here proved to detect asbestos and asbestos-like mineral occurrences, also in limited amount and occurring in thin veins, in fractured and sheared areas of mines and pits. pRS is a promising tool to be used during the in situ phases of the assessment of the risk associated with naturally occurring asbestos and asbestos-like minerals. Mining activities, when operated in asbestos-bearing zones, can take advantage of pRS to identify asbestos occurrences during the front survey and consequently planning the mining operations.

4. Conclusions

pRS has proved to be a reliable, affordable, and easy-to-use instrument for the identification of mineral fibers on the mining front, under several different geological and environmental conditions. Raman spectra acquired with pRS at both low- (bulk modes)

and high-wavenumbers (OH-stretching) had an adequate spectral resolution and signal-to-noise ratio to allow the identification of the main varieties of asbestos and asbestos-like minerals during in situ surveys. In this respect, a portable Raman equipped with a 532-nm laser source and an 8 cm⁻¹ resolution was proved to be able to obtain spectra in the required spectral range (100–4000 cm⁻¹), using a limited amount of time (the instrument is held in contact with the rock by the geologist), on virtually every rock surface. Notably, pRS spectra were of sufficient quality, even in the presence of strongly disaggregated and altered rocks. Fluorescence emission phenomena and the difficulty to focus the laser beam on a non-cohesive bundle of fibers are the main contingencies that can impair the analysis. Relatively easy training for the use and data interpretation is required for operators (e.g., professional geologist).

Supplementary Materials: The following are available online at www.mdpi.com/2076-3417/11/1/287/s1, Figure S1: Schematic for Portable Raman Instrument (pRS); Figure S2: XRPD Qualitative bulk analysis, Figure S3: Representative Raman spectra of non-asbestos phases collected with portable Raman Spectrometer (pRS); Table S1: Assignment of peaks in the Raman spectra at low- and high-wavenumber regions of investigated asbestos and asbestos-like minerals; Figure S4: Raman spectra of a bundle of intermixed chrysotile and fibrous antigorite collected with portable Raman (pRS) and micro-Raman spectrometer (HRS).

Author Contributions: Conceptualization, J.R.P., F.T.; methodology, J.R.P., D.B., F.T.; investigation, J.R.P., M.T., C.L.-M., A.C., D.B.; resources, M.T., C.L.-M., A.C., D.B.; writing—original draft preparation, J.R.P.; writing—review and editing, J.R.P., D.B., E.S.-M., C.L.-M., A.C., F.T.; supervision, C.L.-M., E.S.-M., A.C., D.B., F.T.; funding acquisition, M.T., F.T. All authors have read and agreed to the published version of the manuscript.

Institutional Review Board Statement: Not applicable.

Informed Consent Statement: Not applicable.

Data Availability Statement: The data that support the findings of this study are available from the corresponding author, JRP, upon reasonable request.

Conflicts of Interest: The authors declare no conflict of interest.

References

1. Ross, M.; Nolan, R.P. History of asbestos discovery and use and asbestos-related disease in context with the occurrence of asbestos within ophiolite complexes. *Geol. Soc. Am.* **2003**, 447–470, doi:10.1130/0-8137-2373-6.447.
2. Carbone, M.; Baris, Y.I.; Bertino, P.; Brass, B.; Comertpay, S.; Dogan, A.U.; Gaudino, G.; Jube, S.; Kanodia, S.; Partridge, C.R.; et al. Erionite exposure in North Dakota and Turkish villages with mesothelioma. *Proc. Natl. Acad. Sci. USA* **2011**, *108*, 13618–13623, doi:10.1073/pnas.1105887108.
3. Williams, C.; Dell, L.; Adams, R.; Rose, T.; Van Orden, D.R. State-of-the-science assessment of non-asbestos amphibole exposure: Is there a cancer risk? *Environ. Geochem. Health* **2013**, *35*, 357–377, doi:10.1007/s10653-012-9500-0.
4. IARC. *Monographs on the Evaluation of Carcinogenic Risks to Humans. Arsenic, Metals, Fibres, and Dusts. A Review of Human Carcinogens*; International Agency for Research on Cancer: Lyon, France, 2012; Volume 100C, ISBN 978 92 832 1320 8.
5. IARC. *Monographs on the Evaluation of Carcinogenic Risks to Humans. Fluoro-Edenite, Silicon Carbide Fibres and Whhiskers, and Single-Walled and Multi-Walled Carbon Nanotubes*; International Agency for Research on Cancer: Lyon, France, 2017; Volume 111, ISBN 9789283201779.
6. Harper, M. 10th Anniversary Critical Review: Naturally occurring asbestos. *J. Environ. Monit.* **2008**, *10*, 1394–1408, doi:10.1039/b810541n.

7.   NIOSH. *Asbestos Fibers and Other Elongate Mineral Particles: State of the Science and Roadmap for Research*; National Institute for Occupational Safety and Health: Washington, DC, USA, 2011; Volume 159.

8.   NIOSH. The National Institute for Occupational Safety and Health (NIOSH). Available online: https://www.cdc.gov/niosh/pubs/default.html (accessed on 28 November 2020).

9.   IAEG. Commission NOA EMP Commission—AEG NOA Technical Working Group & IAEG NOA Commission. Available online: http://noa-emp.info/ (accessed on 28 November 2020).

10. INAIL Istituto Nazionale per L'assicurazione Contro gli Infortuni sul Lavoro. Available online: https://www.inail.it/cs/internet/comunicazione/pubblicazioni.html (accessed on 28 November 2020).

11. ANSES. Agence Nationale de Sécurité Sanitaire de L'alimentation, de L'environnement et du Travail. Avis et Rapports de L'ANSES. Available online: https://www.anses.fr/fr/content/avis-et-rapports-de-lanses-sur-saisine (accessed on 28 November 2020).

12. ANSES. *Évaluation de la Toxicité de L'antigorite*; Agence Nationale de Sécurité Sanitaire de l'Alimentation, de l'Environnement et du Travail: Maisons-Alfort, France, 2014.

13. Turci, F.; Tomatis, M.; Gazzano, E.; Riganti, C.; Martra, G.; Bosia, A.; Ghigo, D.; Fubini, B. Potential Toxicity of Nonregulated Asbestiform Minerals: Balangeroite From the Western Alps. Part 2: Oxidant Activity of the Fibres. *J. Toxicol. Environ. Health Part A* **2005**, *68*, 21–39, doi:10.1080/15287390590523911.

14. Gazzano, E.; Riganti, C.; Tomatis, M.; Turci, F.; Bosia, A.; Fubini, B.; Ghigo, D.; Groppo, C.; Tomatis, M.; Turci, F.; et al. Potential Toxicity of Nonregulated Asbestiform Minerals: Balangeroite From the Western Alps. Part 3: Depletion of Antioxidant Defenses. *J. Toxicol. Environ. Health Part A* **2005**, *68*, 41–49, doi:10.1080/15287390590523957.

15. Erskine, B.G.; Bailey, M. Characterization of asbestiform glaucophane-winchite in the Franciscan Complex blueschist, northern Diablo Range, California. *Toxicol. Appl. Pharmacol.* **2018**, *361*, 3–13, doi:10.1016/j.taap.2018.09.020.

16. Di Giuseppe, D.; Harper, M.; Bailey, M.; Erskine, B.; Della Ventura, G.; Ardit, M.; Pasquali, L.; Tomaino, G.; Ray, R.; Mason, H.; et al. Characterization and assessment of the potential toxicity/pathogenicity of fibrous glaucophane. *Environ. Res.* **2019**, *178*, 108723, doi:10.1016/j.envres.2019.108723.

17. Gualtieri, A.F.; Gandolfi, N.B.; Passaglia, E.; Pollastri, S.; Mattioli, M.; Giordani, M.; Ottaviani, M.F.; Cangiotti, M.; Bloise, A.; Barca, D.; et al. Is fibrous ferrierite a potential health hazard? Characterization and comparison with fibrous erionite. *Am. Mineral.* **2018**, *103*, 1044–1055, doi:10.2138/am-2018-6508.

18. Di Giuseppe, D. Characterization of fibrous mordenite: A first step for the evaluation of its potential toxicity. *Crystals* **2020**, *10*, 769, doi:10.3390/cryst10090769.

19. Gualtieri, A.F.; Pollastri, S.; Gandolfi, N.B.; Ronchetti, F.; Albonico, C.; Cavallo, A.; Zanetti, G.; Marini, P.; Sala, O. Determination of the concentration of asbestos minerals in highly contaminated mine tailings: An example from abandoned mine waste of Crètaz and Èmarese (Valle d'Aosta, Italy). *Am. Mineral.* **2014**, *99*, 1233–1247, doi:10.2138/am.2014.4708.

20. Vignaroli, G.; Belardi, G.; Serracino, M. Multi-scale geological evaluation for quarrying activities in ophiolitic rocks: Implications for asbestos-related legislation. *Bull. Eng. Geol. Environ.* **2013**, *72*, 285–302, doi:10.1007/s10064-013-0475-6.

21. Cavallo, A. Environmental asbestos contamination in an abandoned chrysotile mining site: The example of Val malenco (central Alps, northern Italy). *Episodes* **2020**, *43*, 851–858, doi:10.18814/epiiugs/2020/0200s01.

22. Dogan, M.; Emri, S. Environmental health problems related to mineral dusts in Ankara and Eskisehir, Turkey. *Yerbilimleri* **2000**, *22*, 149–161.

23. Cossio, R.; Albonico, C.; Zanella, A.; Fraterrigo-Garofalo, S.; Avataneo, C.; Compagnoni, R.; Turci, F. Innovative unattended SEM-EDS analysis for asbestos fiber quantification. *Talanta* **2018**, *190*, 158–166, doi:10.1016/j.talanta.2018.07.083.

24. Baietto, O.; Marini, P. Naturally occurring asbestos: Validation of PCOM quantitative determination. *Resour. Policy* **2018**, 44–49, doi:10.1016/j.resourpol.2018.06.006.

25. Turci, F.; Avataneo, C.; Botta, S.; Marcelli, I.; Barale, L.; Tomatis, M.; Cossio, R.; Tallone, S.; Piana, F.; Compagnoni, R. New tools for the evaluation of asbestos-related risk during excavation in an NOA-rich geological setting. *Environ. Eng. Geosci.* **2020**, *26*, 113–120, doi:10.2113/EEG-2272.

26. Petriglieri, J.R.; Salvioli-Mariani, E.; Mantovani, L.; Tribaudino, M.; Lottici, P.P.; Laporte-Magoni, C.; Bersani, D. Micro-Raman mapping of the polymorphs of serpentine. *J. Raman Spectrosc.* **2015**, *46*, 953–958, doi:10.1002/jrs.4695.

27. Groppo, C.; Rinaudo, C.; Cairo, S.; Gastaldi, D.; Compagnoni, R. Micro-Raman spectroscopy for a quick and reliable identification of serpentine minerals from ultramafics. *Eur. J. Mineral.* **2006**, *18*, 319–329, doi:10.1127/0935-1221/2006/0018-0319.

28. Rooney, J.S.; Tarling, M.S.; Smith, S.A.F.; Gordon, K.C. Submicron Raman spectroscopy mapping of serpentinite fault rocks. *J. Raman Spectrosc.* **2018**, *49*, 279–286, doi:10.1002/jrs.5277.

29. Rinaudo, C.; Gastaldi, D.; Belluso, E.; Capella, S. Application of Raman spectroscopy on asbestos fibre identification. *Neues Jahrb. fur Mineral.* **2005**, *182*, 31–36, doi:10.1127/0077-7757/2005/0030.

30. Zholobenko, V.; Rutten, F.; Zholobenko, A.; Holmes, A. In situ spectroscopic identification of the six types of asbestos. *J. Hazard. Mater.* **2021**, *403*, 123951, doi:10.1016/j.jhazmat.2020.123951.

31. Rinaudo, C.; Gastaldi, D.; Belluso, E. Characterization of Chrysotile, Antigorite, and Lizardite by FT-Raman Spectroscopy. *Can. Mineral.* **2003**, *41*, 883–890, doi:10.2113/gscanmin.41.4.883.

32. Rinaudo, C.; Belluso, E.; Gastaldi, D. Assessment of the use of Raman spectroscopy for the determination of amphibole asbestos. *Mineral. Mag.* **2004**, *68*, 455–465, doi:10.1180/0026461046830197.

33. Auzende, A.L.; Daniel, I.; Reynard, B.; Lemaire, C.; Guyot, F. High-pressure behaviour of serpentine minerals: A Raman spectroscopic study. *Phys. Chem. Miner.* **2004**, *31*, 269–277, doi:10.1007/s00269-004-0384-0.

34. Tarling, M.S.; Rooney, J.S.; Viti, C.; Smith, S.A.F.; Gordon, K.C. Distinguishing the Raman spectrum of polygonal serpentine. *J. Raman Spectrosc.* **2018**, *49*, 1978–71984, doi:10.1002/jrs.5475.

35. Bard, D.; Tylee, B.; Williams, K.; Yarwood, J. Use of a fibre-optic probe for the identification of asbestos fibres in bulk materials by Raman spectroscopy. *J. Raman Spectrosc.* **2004**, *35*, 541–548, doi:10.1002/jrs.1167.

36. Petriglieri, J.R.; Laporte-Magoni, C.; Gunkel-Grillon, P.; Tribaudino, M.; Bersani, D.; Sala, O.; Le Mestre, M.; Vigliaturo, R.; Gandolfi, N.B.; Salvioli-Mariani, E. Mineral fibres and environmental monitoring: A comparison of different analytical strategies in New Caledonia. *Geosci. Front.* **2020**, *11*, 189–202, doi:10.1016/j.gsf.2018.11.006.

37. Rinaudo, C.; Allegrina, M.; Fornero, E.; Musa, M.; Croce, A.; Bellis, D. Micro-raman spectroscopy and VP-SEM/EDS applied to the identification of mineral particles and fibres in histological sections. *J. Raman Spectrosc.* **2010**, *41*, 27–32, doi:10.1002/jrs.2403.

38. Croce, A.; Musa, M.; Allegrina, M.; Rinaudo, C.; Baris, Y.I.; Dogan, A.U.; Powers, A.; Rivera, Z.S.; Bertino, P.; Yang, H.; et al. Micro-Raman spectroscopy identifies crocidolite and erionite fibers in tissue sections. *J. Raman Spectrosc.* **2013**, *44*, 1440–1445, doi:10.1002/jrs.4286.

39. Bloise, A.; Miriello, D. Multi-Analytical Approach for Identifying Asbestos Minerals In Situ. *Geosciences* **2018**, *8*, 133, doi:10.3390/geosciences8040000.

40. Müntener, O.; Hermann, J.; Trommsdorff, V. Cooling history and exhumation of lower-crutstal granulite and upper mantle (Malenco, Eastern Central Alps). *J. Petrol.* **2000**, *41*, 175–200, doi:10.1093/petrology/41.2.175.

41. Trommsdorff, V.; Montrasio, A.; Hermann, J.; Müntener, O.; Spillmann, P.; Gieré, R. The geological map of Valmalenco. *Schweizerische Mineral. und Petrogr. Mitteilungen* **2005**, *85*, 1–13.

42. Cavallo, A.; Rimoldi, B. Chrysotile asbestos in serpentinite quarries: A case study in Valmalenco, Central Alps, Northern Italy. *Environ. Sci. Process. Impacts* **2013**, *15*, 1341–1350, doi:10.1039/c3em00193h.

43. Adamo, I.; Bocchio, R.; Diella, V.; Pavese, A.; Vignola, P.; Prosperi, L.; Palanza, V. Demantoid from Val Malenco, Italy: Review and update. *Gems Gemol.* **2009**, *45*, 280–287, doi:10.5741/GEMS.45.4.280.

44. Rossetti, P.; Zucchetti, S. Early-alpine ore parageneses in the serpentinites from the Balangero asbestos mine and Lanzo Massif (Internal Western Alps). *Rend. Soc. Ital. Mineral. Petrol.* **1988**, *43*, 139–149.

45. Astolfi, A.; Fubini, B.; Giamello, E.; Volante, M.; Inorganica, C.; Fisica, C.; Torino, U.; Giuria, V. Pietro; Belluso, E.; Ferraris, G. Asbestiform minerals associated with chrysotile from the Western Alps (Piedmont-Italy): Chemical characteristics and possible related toxicity. In *Mechanisms in Fibre Carcinogenisis*; Springer: Boston, MA, USA, 1991; pp. 269–283.

46. Groppo, C.; Tomatis, M.; Turci, F.; Gazzano, E.; Ghigo, D.; Compagnoni, R.; Fubini, B. Potential toxicity of nonregulated asbestiform minerals: Balangeroite from the western Alps. Part 1: Identification and characterization. *J. Toxicol. Environ. Health Part A* **2005**, *68*, 1–19, doi:10.1080/15287390590523867.

47. Troly, G.; Esterle, M.; Pelletier, B.; Reibell, W. Nickel deposits in New Caledonia, some factors influencing their formation. In *Proceedings of the International Laterite Symposium*; American Institute of Mining Metallurgy and Petroleum Engineering Society: New Orleans, LA, USA, 1979; pp. 85–119.

48. Chevillotte, V.; Chardon, D.; Beauvais, A.; Maurizot, P.; Colin, F. Long-term tropical morphogenesis of New Caledonia (Southwest Pacific): Importance of positive epeirogeny and climate change. *Geomorphology* **2006**, *81*, 361–375, doi:10.1016/j.geomorph.2006.04.020.

49. Myagkiy, A.; Truche, L.; Cathelineau, M.; Golfier, F. Revealing the conditions of Ni mineralization in the laterite profiles of New Caledonia: Insights from reactive geochemical transport modelling. *Chem. Geol.* **2017**, *466*, 274–284, doi:10.1016/j.chemgeo.2017.06.018.

50. Maurizot, P.; Sevin, B.; Iseppi, M.; Giband, T. Nickel-bearing laterite deposits in accretionary context and the case of New Caledonia: From the large-scale structure of earth to our everyday appliances. *GSA Today* **2019**, *29*, 4–10, doi:10.1130/GSATG364A.1.

51. Lahondère, D. *Serpentinisation et Fibrogenèse dans les Massifs de Péridotite de Nouvelle-Calédonie. Atlas des Occurrences et des Types de Fibres D'amiante sur Mine*; Bureau de Recherches Géologiques et Minières: Nouméa, Nouvelle Calédonie, 2012.

52. Jehlička, J.; Culka, A.; Bersani, D.; Vandenabeele, P. Comparison of seven portable Raman spectrometers: Beryl as a case study. *J. Raman Spectrosc.* **2017**, *48*, 1289–1299, doi:10.1002/jrs.5214.

53. Compagnoni, R.; Ferraris, G.; Fiona, L. Balangeroite, a new fibrous silicate related to gageite from Balangero, Italy. *Am. Mineral.* **1983**, *68*, 214–219.

54. Bersani, D.; Andò, S.; Scrocco, L.; Gentile, P.; Salvioli-Mariani, E.; Fornasini, L.; Lottici, P.P. Composition of amphiboles in the tremolite–ferro–actinolite series by Raman spectroscopy. *Minerals* **2019**, *9*, 491, doi:10.3390/min9080491.

55. Groppo, C.; Compagnoni, R. Metamorphic veins from the serpentinites of the Piemonte Zone, western Alps, Italy: A review. *Period. Mineral.* **2007**, *76*, 127–153, doi:10.2451/2007PM0021.